Calibration of the Characteristic Frequency of an Optical Tweezer using a Recursive Least-Squares Approach

Aruna Ranaweera
ranawera@engineering.ucsb.edu

Bassam Bamieh
bamieh@engineering.ucsb.edu

Department of Mechanical and Environmental Engineering, University of California, Santa Barbara, CA 93106-5070

***Abstract*— We describe the use of a Recursive Least-Squares approach for calibration of the characteristic frequency of an optical tweezer. Unlike commonly used off-line calibration methods, the RLS algorithm does not require data averaging to reduce the effects of Brownian motion. We use computer simulations to demonstrate that the RLS algorithm can be used to efficiently calibrate the characteristic frequency of a trapped, 10-micron diameter polystyrene bead. However, experimental results suggest that applying the RLS method to an actual optical tweezer system is more difficult because of measurement errors and laboratory noise.**

I. Introduction

The optical tweezer is a device that uses a focused laser beam to trap and manipulate individual dielectric particles in an aqueous medium. The laser beam is sent through a high numerical aperture (highly converging) microscope objective that is used for both trapping and viewing particles of interest. For small enough displacements from the center of the trap, the optical tweezer behaves like a Hookeian spring, characterized by a fixed trap-stiffness.

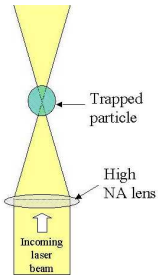

Fig. 1. Optical Tweezer. A single laser beam is focused to a diffraction-limited spot using a high numerical aperture microscope objective. Dielectric particles are trapped near the laser focus.

Several milliwatts of laser power at the focus can generate trapping forces on the order of piconewtons. While tiny by conventional standards, this level of force is well suited for biomolecular studies. Although biological molecules are too small to be trapped at room temperature, a molecule can be grasped once a trappable 'handle', such as a polystyrene bead, is (biochemically) attached to that molecule [1].

The optical tweezer is a controllable *actuator* at the piconewtons scale. In experiments that investigate the forces that arise due to various (usually biological) interactions, the trapping forces must be accurately quantified. Since strongest trapping occurs when trapped particles are roughly the same size as the laser wavelength, most biological experiments are performed in this size regime [2]. However, the absence of an accurate theoretical model for trapping behavior in this regime means that the capability of an optical tweezer is almost always quantified empirically [3]. The trapping capability of an optical tweezer can be quantified by its characteristic frequency ω_c which is defined as the ratio of trap stiffness to viscous damping.

Although calibration can be performed off-line using either step response data or power spectrum data, such methods are inherently slow because they require averaging to reduce the effects of Brownian (thermal) motion [3], [4]. Attempts to calibrate using a Normalized Gradient (NG) algorithm are also severely hampered by thermal noise [3].

In the remaining sections of this paper, we use a well-known Recursive Least Squares (RLS) algorithm, which does not require averaging, to obtain significantly faster calibration of the characteristic frequency. Computer simulations and experimental results are included.

II. Equation of Motion

The equation of motion along the lateral x-axis for a trapped bead of mass m and lateral position x is given by

$$m\ddot{x} = F_T(x_r) + F_D(\dot{x}) + F_L(t) + F_E(t), \qquad (1)$$

where $F_T(\cdot)$ is the optical trapping force, $F_D(\cdot)$ is the viscous drag, $F_L(\cdot)$ is a Langevin (random thermal) force, and $F_E(\cdot)$ is an external driving force. The relative displacement x_r is defined as $x_r := x - x_T$, in which x_T is trap position. Within the linear radius of $|x_r| < R_l$, the trap stiffness is approximately constant and the trapping force is linear with respect to relative displacement:

$$F_T = -\alpha x_r. \qquad (2)$$

For a 1-μm diameter polysyrene bead, $R_l \approx 0.2$ μm [5]. The linear radius increases with bead size. The drag force can be expressed as

$$F_D = -\beta \dot{x}, \qquad (3)$$

where $\beta > 0$ is the viscous damping factor from Stoke's equation, $\beta = 6\pi\eta r$, in which r is the bead radius and η is the fluid viscosity. For a 10-μm diameter polystyrene bead in water at 20°C, $m = 5.2 \times 10^{-7}$ mg and $\beta \approx 0.1$ $\frac{\text{pNs}}{\mu\text{m}}$. The Langevin force has an average value of zero, $E\{F_L(t)\} = 0$, and constant power spectrum $S_L(f)$ (i.e., ideal white noise force) given by

$$S_L(f) = 4\beta k_B T, \tag{4}$$

in which k_B is Boltzmann's constant and T is the absolute temperature [6]. At biological temperatures, $k_B T$ is approximately 4×10^{-3} pNμm [6]. Therefore, for a 10-μm diameter polystyrene bead, $S_L(f) \approx 1.6 \times 10^{-3}$ $\frac{\text{pN}^2}{\text{Hz}}$. The nature of the external force $F_E(t)$ will depend on experimental conditions. For example, in biological experiments, the external force will arise due to the interaction between the trapped bead and biological particles.

Assuming the particle mass is negligible compared to the viscous drag, (1),(2), and (3) can be combined to obtain the noninertial equation of motion for a trapped particle in the linear trapping region:

$$0 = -\alpha x_r - \beta \dot{x} + F_L(t) + F_E(t). \tag{5}$$

The characteristic frequency of the trap (in radians per second) is defined as

$$\omega_c := \frac{\alpha}{\beta}. \tag{6}$$

A. Transfer Functions

Defining trap position as the control input, $u := x_T$, and using (6), (5) can be written in state space form as

$$\begin{aligned} \dot{x} &= -\omega_c x + \omega_c u + \frac{1}{\beta} F_L + \frac{1}{\beta} F_E \\ y &= x. \end{aligned} \tag{7}$$

Defining Langevin disturbance $d_L := F_L$, and external disturbance $d_E := F_E$, and assuming zero initial conditions, (7) can be expressed using Laplace transforms as:

$$X(s) = G_{yu}(s)U(s) + G_{yd}(s)\left[D_L(s) + D_E(s)\right], \tag{8}$$

in which the first order transfer functions are given by

$$G_{yu}(s) = \frac{\omega_c}{s + \omega_c} \tag{9}$$

and

$$G_{yd}(s) = \frac{\frac{1}{\beta}}{s + \omega_c}. \tag{10}$$

A schematic block diagram of the linear plant P is shown in Figure 2.

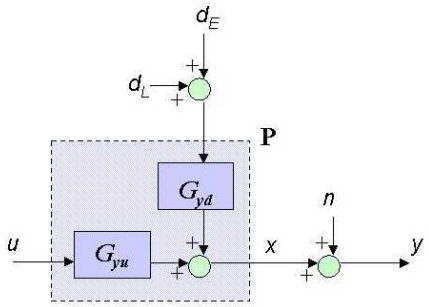

Fig. 2. Linear plant block diagram, in which $u := x_T$, $d_L := F_L$, $d_E := F_E$, and n is measurement noise.

B. Zero-Order-Hold Representations

A continuous-time (CT) scalar system of the form

$$\begin{aligned} \dot{x} &= -ax + bu \\ y &= x \end{aligned} \tag{11}$$

with corresponding transfer function

$$G(s) = \frac{b}{s + a} \tag{12}$$

can be zero-order hold sampled with sampling time h to obtain the discrete-time (DT) system

$$\begin{aligned} x(kh + h) &= -a_1 x(kh) + b_1 u(kh) \\ y(kh) &= x(kh), \end{aligned} \tag{13}$$

where k is a positive integer and

$$\begin{aligned} a_1 &= -e^{-ah} \\ b_1 &= \frac{b}{a}\left(1 - e^{-ah}\right) \end{aligned} \tag{14}$$

[7]. The sampled-system can also be represented by the difference equation $y(kh) = H(q)u(kh)$, where $H(q)$ is the pulse transfer operator given by

$$H(q) = \frac{b_1}{q + a_1}, \tag{15}$$

in which q is the forward shift operator [7]. From (14), if we use a DT identification algorithm to obtain DT parameter estimates $\widehat{a}_1$ and $\widehat{b}_1$, the corresponding CT parameter estimates $\widehat{a}$ and $\widehat{b}$ are given by

$$\begin{aligned} \widehat{a} &= -\frac{1}{h}\ln(-\widehat{a}_1) \\ \widehat{b} &= -\left(\frac{\widehat{b}_1}{1 + \widehat{a}_1}\right)\frac{1}{h}\ln(-\widehat{a}_1). \end{aligned} \tag{16}$$

From (14) and (15), the zero-order hold equivalent of $G_{yu}(s)$ in (9) is given by

$$H_{yu}(q) = \frac{1 - e^{-\omega_c h}}{q - e^{-\omega_c h}}. \tag{17}$$

For example, for $h = 0.001$ s, $\omega_c = 78$ rad/s gives $G_{yu}(s) = \frac{78}{s+78}$ and therefore $H_{yu}(q) = \frac{0.07504}{q-0.9250}$, whereas $\omega_c = 65$ rad/s gives $G_{yu}(s) = \frac{65}{s+65}$ and $H_{yu}(q) = \frac{0.07653}{q-0.9242}$. Note that the DT parameters a_1 and b_1 are relatively insensitive to variations in the continous parameters ω_c. In particular, from (15) and (17), we obtain

$$\frac{da_1}{d\omega_c} = \frac{db_1}{d\omega_c} = he^{-\omega_c h}, \tag{18}$$

which is just under 0.001 for the values chosen above.

III. Recursive Least Squares Algorithm

In this section, we will use the sampling time h as the unit of time. We would like to compute the DT parameter estimate $\widehat{\theta}(k) := [\widehat{a}_1 \quad \widehat{b}_1]^T$ at sample k that minimizes the weighted least-squares criterion:

$$\widehat{\theta}(k) = \overset{\min}{\theta} \sum_{n=1}^{k} w(k,n)[y(n) - \phi^T(n)\theta]^2, \tag{19}$$

where $\phi(k) := [-y(k-1) \quad u(k-1)]^T$ is the regression vector that contains the input and output data, and $w(k,n)$ is a weighting sequence with the property,

$$\begin{aligned} w(k,n) &= \lambda(k)w(k-1,n), \quad 0 \le n \le k-1 \\ w(k,k) &= 1, \end{aligned} \tag{20}$$

in which $\lambda(k)$ is the forgetting factor [4]. The RLS algorithm is given by

$$\begin{aligned} \widehat{\theta}(k) &= \widehat{\theta}(k-1) + \\ &\quad L(k)\left[y(k) - \phi^T(k)\widehat{\theta}(k-1)\right] \end{aligned} \tag{21}$$

$$L(k) = \frac{P(k-1)\phi(k)}{\lambda(k) + \phi^T(k)P(k-1)\phi(k)} \tag{22}$$

$$\begin{aligned} P(k) &= \frac{1}{\lambda(k)}\left[P(k-1) - \right. \\ &\quad \left. \frac{P(k-1)\phi(k)\phi^T(k)P(k-1)}{\lambda(k) + \phi^T(k)P(k-1)\phi(k)}\right], \end{aligned} \tag{23}$$

where

$$P(k) := \left[\sum_{n=1}^{k} w(k,n)\phi(n)\phi^T(n)\right]^{-1} \tag{24}$$

is the scaled covariance matrix of the parameters at sample k. The initial parameter vector is denoted as $\widehat{\theta}(0) = \theta_0$ and the initial covariance matrix is denoted as $P(0) = P_0$. In other words, θ_0 is what we guess the parameter vector to be before seeing the data, and P_0 reflects our confidence in this guess [4]. The initial regression vector is specified as $\phi(0) = [0 \quad 0]^T$. The forgetting factor λ is constant for a slowly changing system and can be chosen according to

$$\lambda = 1 - \frac{1}{K}, \tag{25}$$

where K is the memory time constant. Data older than K samples are weighted by a factor $e^{-1} \approx 36\%$ compared to the most recent data [4]. For an LTI system, it is natural to require that all data be given equal weight, which implies that no data is discounted. By setting $K \to \infty$ in (25), we obtain $\lambda = 1$.

IV. Computer Simulations

The CT system described by (8) was simulated using *Simulink* with a simulation sampling time of $T_s = 0.1$ ms, corresponding to 10 kilosamples per second (kS/s). The Langevin disturbance was modeled as band-limited white noise with bandwidth 10 kHz and constant power $S_L(f) = 1.6 \times 10^{-3} \ \frac{\text{pN}^2}{\text{Hz}}$. As mentioned in Section II, this represents the Langevin force that acts on a 10-μm diameter polystyrene bead at biological temperatures. To facilitate comparison with experimental results in Section V, the actual characteristic frequency of the simulated system is chosen as $\omega_c = 78$ rad/s. According to Section II-B, for RLS sampling time $h = 1$ ms, the actual parameters are given by

$$a = b = 78 \tag{26}$$

and

$$\theta = \begin{bmatrix} a_1 \\ b_1 \end{bmatrix} = \begin{bmatrix} -0.925 \\ 0.07504 \end{bmatrix}. \tag{27}$$

To enable quantitative comparisons with the results from [3], we assume an initial characteristic frequency guess of $\widehat{\omega}_c(0) = 65$ rad/s, which corresponds to an error of 20% (13 rad/s). According to Section II-B, the initial parameter conditions are given by

$$\widehat{a}(0) = \widehat{b}(0) = 65 \tag{28}$$

and

$$\theta_0 = \begin{bmatrix} \widehat{a}_1(0) \\ \widehat{b}_1(0) \end{bmatrix} = \begin{bmatrix} -0.9242 \\ 0.07653 \end{bmatrix}. \tag{29}$$

For invertibility, we assume the initial covariance matrix is of the form

$$P_0 = \begin{bmatrix} p & 0 \\ 0 & p \end{bmatrix},$$

in which $p > 0$. In the simulations that follow, we will denote the input signal amplitude by A and input frequency by f.

Figure 3 shows results for an input square wave with $A = 0.2$ μm and $f = 10$ Hz. The top plot shows the input and output (I/O) signals, the middle plot shows the DT parameter estimates, and the bottom plot shows the CT parameter estimates. For comparison, the DT estimates are plotted as $1 + \widehat{a}_1$ and $\widehat{b}_1$, since, according to (14), we would like these two quantities to converge to the same value ($= b_1$).

After fluctuating wildly at the onset, both the DT and CT parameter estimates eventually converge close to the correct values of b_1 and ω_c, respectively. The simulation is shown on an expanded time scale in Figure 4, in which the $\omega_c \pm 5\%$ and $\omega_c \pm 2\%$ limits are included in the bottom plot.

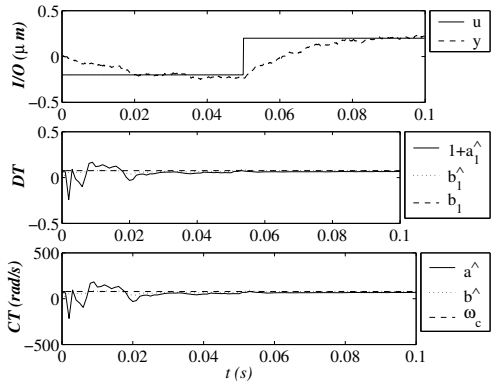

Fig. 3. Simulation of RLS for $h = 1$ ms, $\lambda = 1$, $p = 10^4$; square wave input, $A = 0.2$ μm and $f = 10$ Hz.

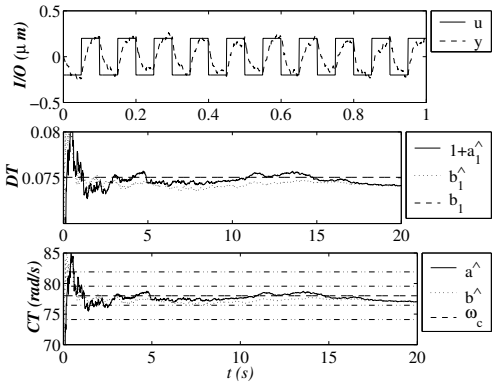

Fig. 4. Simulation of RLS for $h = 1$ ms, $\lambda = 1$, $p = 10^4$; square wave input, $A = 0.2$ μm and $f = 10$ Hz. Dash-dotted lines on the bottom plot show $\omega_c \pm 5\%$ and $\omega_c \pm 2\%$ limits.

Although the parameter estimates display small fluctuations that do not disappear with time, the CT parameter estimates settle to within 5% of ω_c in under 0.6 s and to within 2% in under 8 seconds. The direct correspondence between the DT and CT estimates can be seen from the similar shape of their plots. As shown in (18), fluctuations in the DT estimates will amplify the CT estimates by a factor of over 1000. The reason for the paramater fluctuations is the Langevin disturbance. This is demonstrated by Figure 5, which is a hypothetical simulation for zero Langevin disturbance.

No oscillations are observed and the CT parameter estimates settle to within 5% of ω_c in under 3 ms (3 iterations) and to within 2% in under 4 ms (4 iterations).

A. Effect of Input Signal Parameters

1) Input Frequency: We found that both $f = 2$ Hz and $f = 20$ Hz resulted in slower parameter convergence. The value of $f = 10$ Hz was used because it gave the fastest convergence for the chosen value of ω_c. This is consistent with the practical recommendation that input power be selected at frequency bands in which a "good model is particularly important", or

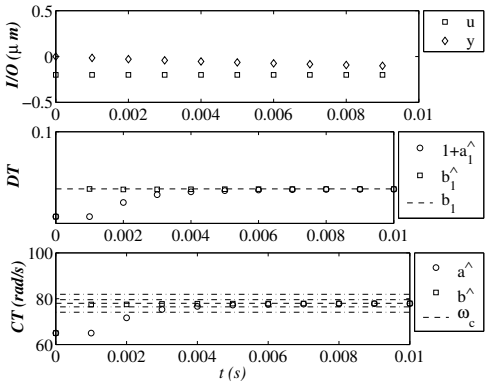

Fig. 5. Hypothetical $F_L = 0$ simulation of RLS for $h = 1$ ms, $\lambda = 1$, $p = 10^4$; square wave input, $A = 0.2$ μm and $f = 10$ Hz.

more formally, frequencies at which the "Bode plot is sensitive to parameter variations" [4]. The optimal input frequency for $\omega_c = 78$ rad/s is $f \approx 12$ Hz, which is close to 10 Hz.

2) Input Shape: We found that a square wave provides faster convergence than both a sinusoidal input ($f = 10$ Hz) and a random input. Furthermore, we found that random input signals yield erroneous paramater estimates. The superiority of the square wave can be explained using the crest factor C_r, which should be minimized to reduce the covariance of the parameter estimates [4]. For a discrete input sequence $\{u(k)\}$, the crest factor is given by

$$C_r^2 = \frac{\max_k u^2(k)}{\lim_{N\to\infty} \frac{1}{N} \sum_{k=1}^{N} u^2(k)}, \qquad (30)$$

which is clearly at its theoretical lower bound for binary, symmetric signals such as a square wave [4].

B. Effect of RLS Algorithm Parameters

1) Forgetting Factor: According to (25), a forgetting factor of $\lambda = 0.9999$ corresponds to a memory time constant of $K = 10000$ samples, which is equivalent to $t = 10$ s for $h = 1$ ms. Figure 6 shows simulation results for $\lambda = 0.9999$.

The CT parameter estimates settle to within 5% of ω_c in under 0.6 s, but they do not settle within the 2% limit. Clearly, the parameter estimates fluctuate more for the $\lambda = 0.9999$ case than for the $\lambda = 1$ case shown in Figure 4. Intuitively, since the past data is exponentially discounted with time, there is less smoothing of the past data. Therefore, the identification algorithm is more sensitive to the Langevin disturbance and the convergence properties are diminished.

2) Initial Covariance Matrix: By decreasing initial covariance matrix gain from $p = 10^4$ to $p = 1$, we can specify greater confidence in our initial parameter guess. Figure 7 shows simulation results for $p = 1$.

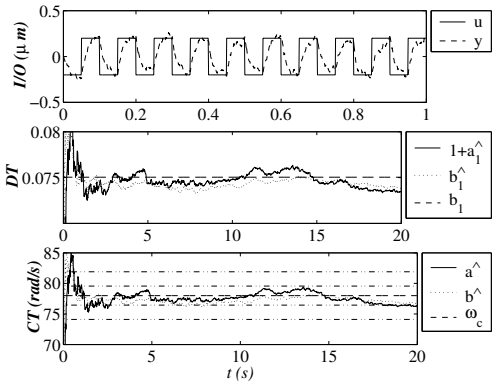

Fig. 6. Simulation of RLS for $h = 1$ ms, $\lambda = 0.9999$, $p = 10^4$; square wave input, $A = 0.2$ μm and $f = 10$ Hz.

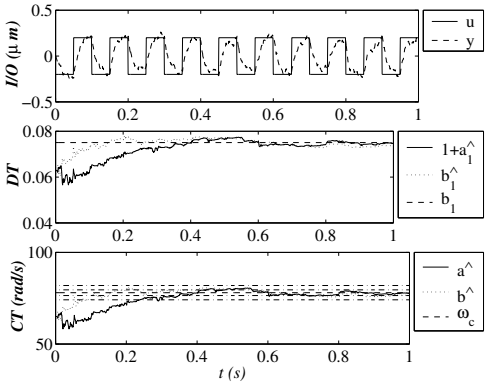

Fig. 7. Simulation of RLS for $h = 1$ ms, $\lambda = 1$, $p = 1$; square wave input, $A = 0.2$ μm and $f = 10$ Hz.

Comparing with Figure 3, we see that the smaller value of p results in significantly smaller initial fluctuations in the parameter estimates. Further simulations show that, for $p = 1$, the CT parameter estimates settle to within 5% of ω_c in under 0.3 s and to within 2% in under 8.5 s, which are similar to the settling times for $p = 10^4$.

It should be mentioned that, since the RLS algorithm is implemented using a PC, the input and output position amplitudes can be scaled if necessary (within computation limits), but this does not affect convergence times for the RLS algorithm, so the data was not scaled.

V. Experimental Results

A schematic diagram of our single-axis optical tweezer system is shown in Figure 8 [3].

Since the RLS algorithm does not require real-time feedback control, we were able to investigate its performance by collecting input and output data from our system using *LabVIEW* data acquisition software and hardware and then processing the data using *Matlab* [3]. Data was sampled at a rate of 2 kS/s with an analog lowpass filter at the Nyquist frequency. Figure 9 shows

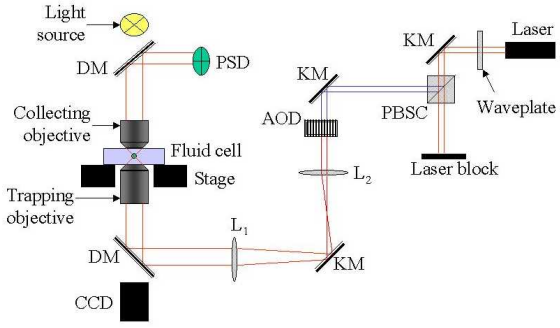

Fig. 8. Schematic diagram of single-axis optical tweezer system. PBSC = Polarizing Beam Splitting Cube, KM = Kinematic Mirror, AOD = Acousto-Optic Deflector, PSD = Position Sensing Detector, CCD = CCD Camera, DM = Dichroic Mirror.

results for an input square wave with $A = 0.2$ μm and $f = 10$ Hz.

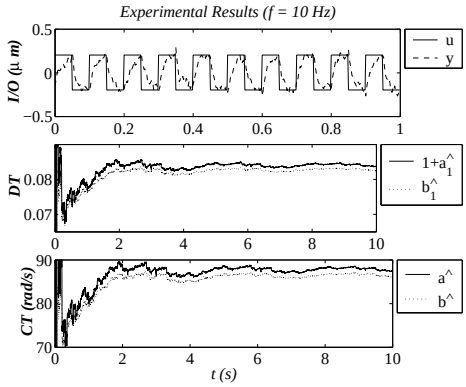

Fig. 9. Implementation of RLS for experimental data with $h = 1$ ms, $\lambda = 1$, $p = 10^4$; square wave input, $A = 0.2$ μm and $f = 10$ Hz.

After initial fluctuations, the parameter estimates appear to reach steady values within 9 seconds. The values of the CT estimates after 10 s are $\widehat{a} = 88$ rad/s and $\widehat{b} = 86$ rad/s. The slight disparity between these two estimates is likely due to attenuation from the lowpass filter. The parameter convergence values for different input frequencies are shown in Table I, including the two off-line methods. The RLS results are for 10 seconds of data, while the off-line results are for the average of 30 seconds of data [3]. The RLS parameter estimates are not consistent with the results for off-line calibration methods such as the power spectrum and step response [3]. Further implementation shows that for lower frequencies ($f = 2$ Hz and $f = 5$ Hz), the RLS algorithm does not converge to steady values within 10 s. As shown in Section IV, this is almost certainly due to the mismatch in input frequency and the characteristic frequency of the system. The result is slower convergence for lower input frequencies.

The inconsistencies can be due to several factors. For example, even slight misalignments in the position

Calibration method	$\widehat{a}$	$\widehat{b}$	Convergence after 10 s
RLS (f = 2 Hz)	85	82	Unsteady
RLS (f = 5 Hz)	89	85	Unsteady
RLS (f = 10 Hz)	88	86	Steady
Power Spectrum	75	75	
Step Response	78	78	

TABLE I

PARAMETER ESTIMATES FOR EXPERIMENTAL DATA.

detection system and fluctuations in the dynamic laser pointing system (the AOD) can cause systematic errors that distort the RLS calibration results. The power spectrum method, in particular, is robust with respect to such factors [6], [8]. Additional sources of measurement noise, such as low-frequency drift and other types of electronic bias, high frequency amplifier noise, mechanical vibrations, and extraneous background light can also contribute to erroneous estimates. Such problems are inherent in any practical position detection system. The presence of an analog RC lowpass filter can also distort the RLS calibration results. However computer simulations show that the typical effect of the lowpass filter is to reduce the parameter estimates, not increase them. Therefore, it is unlikely that the lowpass filter caused the disparities in Table I.

In light of the disparities between the results shown in Table I, more analysis and experimental work needs to be done before we can make definitive quantitative claims about the convergence of the RLS algorithm when applied to typical experimental data.

VI. CONCLUSION

This paper describes the calibration of the characteristic frequency of an optical tweezer using a well-known recursive least-squares approach. For a system with characteristic frequency of approximately 12 Hz, we use computer simulations to show that a square wave input with frequency 10 Hz can be used to estimate the parameters to within 5% accuracy in under 1 s and to within 2% accuracy in under 10 s. We also demonstrate that initial parameter fluctuations can be significantly decreased by reducing the initial covariance matrix, but this does not appear to improve steady state convergence times. We find that convergence properties are diminished for forgetting factors less than 1.

For a system–such as an optical tweezer–that is subject to a large stochastic disturbance, the RLS method is, in theory, superior to an on-line identification method such as the NG algorithm, which is not designed to handle large disturbances. In fact, computer simulations show that the RLS algorithm is at least one order of magnitude faster than the NG algorithm [3]. In practice, the characteristic frequency of an optical trap can vary due to laser fluctuations, local heating, and cross-contamination. Methods that depend on purely off-line data analysis do not account for these effects and may suggest an erroneous value for the characteristic frequency. Therefore, in a laboratory environment in which experimental conditions are not entirely constant, the RLS algorithm could potentially provide a more reliable (up-to-date) measure of characteristic frequency than the off-line methods that are widely in use. Furthermore, since the RLS algorithm is specifically designed for on-line identification, it is easy to implement using a PC.

Our experimental results are not consistent with previous, off-line calibration results. Although the RLS parameter estimates converge for an input frequency of 10 Hz, the estimates are about 12% greater than the off-line values. Further analysis is needed before the RLS method can be recommended for accurate calibration of experimental results. In light of the effectiveness of the RLS method when applied to computer generated data, it is very likely that the experimental difficulties can be overcome by reducing laboratory noise and increasing the accuracy of our position detection system.

Also, the results of this paper pertain specifically to a 10-μm diameter polystyrene bead trapped in water at biological temperature. The characteristic frequency for a 1-μm bead will be at least 10 times larger, whereas the Langevin noise power will be one-tenth. In future work, we will investigate the performance of the RLS algorithm for a 1-μm bead, which is widely used in biophysics.

It should be pointed out that this paper only considers calibration of the characteristic frequency ω_c. If specific information about stiffness α and drag β are sought, the off-line power spectrum method is unrivalled in many aspects [6]. However, due to its speed and ease of implementation, we believe that the RLS algorithm described here will prove to be a useful tool for users of optical tweezers.

REFERENCES

[1] S. Chu, "Laser manipulation of atoms and particles," *Science*, vol. 253, pp. 861–866, 1991.

[2] A. D. Mehta, J. T. Finer, and J. A. Spudich, "Reflections of a lucid dreamer: optical trap design considerations," in *Methods in Cell Biology* (M. P. Sheetz, ed.), vol. 55, ch. 4, pp. 47–69, Academic Press, 1998.

[3] A. Ranaweera and B. Bamieh, "Calibration of the characteristic frequency of an optical tweezer using an adaptive normalized gradient approach," in *Proceedings of the 2003 American Control Conference*, (Denver, CO), pp. 3738–3743, IEEE, June 2003.

[4] L. Ljung, *System Identification*. Prentice Hall PTR, 2nd ed., 1999.

[5] R. M. Simmons, J. T. Finer, S. Chu, and J. Spudich, "Quantitative measurements of force and displacement using an optical trap," *Biophys. J.*, vol. 70, pp. 1813–1822, 1996.

[6] F. Gittes and C. H. Schmidt, "Signals and noise in micromechanical measurements," in *Methods in Cell Biology* (M. P. Sheetz, ed.), vol. 55, ch. 8, pp. 129–156, Academic Press, 1998.

[7] K. J. Astrom and B. Wittenmark, *Computer-Controlled Systems*. Prentice Hall, 3rd ed., 1997.

[8] K. Visscher, S. P. Gross, and S. M. Block, "Construction of multiple-beam optical traps with nanometer-resolution position sensing," *IEEE J. Select. Topics Quantum Electronics*, vol. 2, no. 4, pp. 1066–1076, 1996.